



Geophysical Research Letters*

RESEARCH LETTER

10.1029/2021GL096970

Key Points:

- Global hybrid model predicts that hot flow anomalies (HFAs) generally exhibit north-south and dawn-dusk global asymmetries due to the 3-D bow shock geometry
- HFAs generated by tangential discontinuity impact only appear in one hemisphere even when electric fields point inwards in both hemispheres
- The north-south global HFA asymmetry is driven by a reversal in the north-south component of ion velocity across the equatorial bow shock

Supporting Information:

Supporting Information may be found in the online version of this article.

Correspondence to:

Y. Lin, linyu01@auburn.edu

Citation:

Lin, Y., Wang, X., Sibeck, D. G., Wang, C.-P., & Lee, S.-H. (2022). Global asymmetries of hot flow anomalies. *Geophysical Research Letters*, 49, e2021GL096970. https://doi. org/10.1029/2021GL096970

Received 8 NOV 2021 Accepted 7 FEB 2022

Global Asymmetries of Hot Flow Anomalies

Yu Lin¹, Xueyi Wang¹, David G. Sibeck², Chih-Ping Wang³, and Sun-Hee Lee⁴

¹Physics Department, Auburn University, Auburn, AL, USA, ²NASA Goddard Space Flight Center, Greenbelt, MD, USA, ³Department of Atmospheric and Oceanic Sciences, University of California, Los Angeles, CA, USA, ⁴Catholic University of America, Washington, DC, USA

Abstract A three-dimensional global hybrid simulation is conducted for the interaction of the Earth's bow shock with an interplanetary directional tangential discontinuity (TD) whose normal lies in the equatorial plane. Although the convection electric field points into the TD from its trailing side both north and south of the equator, the interaction only generates a hot flow anomaly (HFA) in the southern hemisphere. HFA generation results from bow shock-reflected ions energized by the inward-pointing electric field on one side of the TD and inward ion gyration on the other side. The latter only occurs south of the equator due to the global bow shock geometry. The global HFA asymmetry is driven by a reversal in the north-south component of reflected ion velocities in the two hemispheres, such that ions gyrate into (away from) the TD in the southern (northern) hemisphere. Our results indicate HFAs must generally exhibit north-south and dawn-dusk asymmetries.

Plain Language Summary Interplanetary magnetic field (IMF) discontinuities frequently occur in the solar wind. When interplanetary tangential discontinuities (TDs) interact with the terrestrial bow shock, localized large-amplitude transient structures known as hot flow anomalies (HFAs) can be generated and cause significant perturbations in the magnetosphere, even though the pristine TD exhibits no plasma variations. Previous studies based on satellite observations and global hybrid simulations suggest that HFAs occur when convection electric fields point toward the TD on at least one side, a condition under which the bow shock ions are likely to be injected and accumulated in the TD. The previous global simulations, however, were based on 2-D assumptions. In this paper, we conduct a 3-D global hybrid simulation for the interaction of the bow shock with an interplanetary directional TD, in which the IMF is symmetric about the equator on both sides of the TD. Although the convection electric field points into the TD from one side of the discontinuity at locations both north and south of the equator, the interaction only generates an HFA in the southern hemisphere. By examining ion velocity distributions, a mechanism is proposed for the global asymmetry of the HFA. Our simulation indicates that HFAs must generally exhibit north-south and dawn-dusk asymmetries.

1. Introduction

When interplanetary discontinuities impact the terrestrial bow shock, significant perturbations in plasma density, temperature, and velocity can be generated due to kinetic processes associated with energetic solar wind ions, even when the original discontinuity exhibits no plasma variations (Archer et al., 2012; Lin et al., 1996; Sibeck et al., 1999). Among these structures, hot flow anomalies (HFAs) observed near the bow shock are large-amplitude transient structures characterized by hot subsonic plasma cores with low magnetic fields and low plasma densities, accompanied by significant transient flow deflections and usually flanked by narrow regions of high density and strong magnetic field (Schwartz, 1995; Thomsen et al., 1986; Zhang et al., 2010). Most HFAs are associated with a variation in the interplanetary magnetic field (IMF) direction (Paschmann et al., 1988; Sibeck et al., 1999), generally a directional interplanetary tangential discontinuity (TD) that carries an IMF direction change (Facskó et al., 2008; Lucek et al., 2004; Schwartz et al., 1988; Thomsen et al., 1993; Zhang et al., 2010).

Analyses based on satellite observations suggest that HFAs are generated when convection electric fields point toward the TD on at least one side (Schwartz et al., 2000; Zhao et al., 2017), a condition under which the bow shock ions are likely to be injected and accumulated in the TD. A theoretical mechanism consistent with observations was first demonstrated with a test-particle simulation for a static convecting TD (Burgess, 1989) and then with local-scale hybrid simulations (Thomas et al., 1991). Two-dimensional (2-D) global hybrid simulations of Lin (1997, 2002) for the interaction of TDs with the bow shock show that, indeed, HFAs (and their magnetosheath counterparts Hasegawa et al., 2012) can be generated when TDs exhibit inward-pointing electric fields to accelerate the bow shock-reflected ions. HFAs formed in these simulations can reduce pressures so much

© 2022. American Geophysical Union. All Rights Reserved.

LIN ET AL. 1 of 9



that the magnetosheath and magnetopause expand sunward significantly. The multispacecraft event reported by Sibeck et al. (1999) has revealed that the interaction of an interplanetary TD and the bow shock led to an HFA, in which the pressures decreased by an order of magnitude. The magnetopause bulged sunward, resulting in a sudden auroral brightening. Significant magnetopause expansions caused by HFAs have also been reported by Eastwood et al. (2008) and Jacobsen et al. (2009). Understanding the conditions under which HFAs occur is important because these transients produce drastic impulses in the magnetosheath, magnetopause (Archer et al., 2012), and trigger global ULF wave activity in the magnetosphere (Zhao et al., 2017).

HFAs occur at both quasi-perpendicular (Q- \perp) and quasi-parallel (Q- \parallel) shocks (Facskó et al., 2009; Schwartz et al., 2000; S. Wang et al., 2013). Global hybrid simulations of Omidi and Sibeck (2007) and Omidi et al. (2013) illustrated the formation of HFAs and spontaneous HFAs (Omidi et al., 2013; Zhang et al., 2013) at the Q- \parallel shock, where a significant percentage of foreshock ions can interact with an interplanetary TD. Other studies further suggest that when the convection electric field points toward the TD, the Hall current from demagnetized foreshock ions enables the growth of the HFA (Liu et al., 2020). S. Wang et al. (2013), however, showed that the presence of an inward-pointing electric field is not a necessary condition for the presence of an HFA.

Previous global simulations involving HFAs, however, were performed with 2-D models. The extended global distribution and thus impacts of HFAs over the 3-D magnetopause are still inadequately understood. This paper uses the Auburn Global Hybrid Code in 3-D (ANGIE3D) to demonstrate that the generation of HFAs from the bow shock-TD interaction has a general and significant global north-south (and dawn-dusk) asymmetry even when symmetry about the equator (noon meridian plane) might be expected, and this asymmetry results from ion gyro orbits in the 3D geometry of the bow shock. Ion gyro motions have also been linked to the strong global north-south asymmetry in plasma environments beyond the Earth (Delamere, 2006). Our simulation indicates that the impact of HFAs may be far more complex than conventional mechanisms predict. We describe our global hybrid model in Section 2, and the simulation results in Section 3. A summary and discussion are given in Section 4.

2. 3-D Global Hybrid Simulation Model

The global hybrid code ANGIE3D (Cheng et al., 2020; Lin et al., 2014, 2017) has been used for simulations of the magnetotail as well as the foreshock bubbles resulting from the interaction between the bow shock and an interplanetary rotational discontinuity (C. P. Wang et al., 2020) or TD (C. P. Wang et al., 2021a). The 3-D simulation domain is bounded by the outer planes of x = +25 R_E and -60 R_E , y = +60 R_E and -35 R_E , and z = +35 R_E and -45 R_E in the GSM coordinate system, and an inner edge at $z \approx 3.0$ $z \approx 1.0$ S.

The initial IMF is assumed to be $\mathbf{B}_0 = (3.0, 1.7, 0)$ nT. The solar wind flow velocity is $\mathbf{V}_0 = (-400, 0, 0)$ km/s. We present the simulation corresponding to a solar wind ion density of 5/c. c., with an ion temperature of 10 eV and an electron-to-ion temperature ratio of 0.1. The solar wind ion inertial length d_{i0} is chosen to be 0.1 R_E . The cell dimensions are $n_x \times n_y \times n_z = 502 \times 507 \times 400$. Nonuniform cell grids comparable to the local d_i values are used, with grid size equal to 0.12 and 0.15 R_E in each direction in the magnetosheath and the bow shock/foreshock, respectively. Since d_{i0} (and thus the Alfveń speed) assumed is larger by a factor of 6.2 than the realistic values, we scale time by a factor of 6.2 (Lin et al., 2014).

After the bow shock and magnetosphere form self-consistently under the initial conditions, a TD propagates into the domain from the upstream boundary with a half width of $0.12\,R_E$, which then evolves self-consistently while propagating. Behind (i.e., on the sunward side of) the TD, the IMF changes to $\mathbf{B}_1 = (0, 0, -3.4)$ nT, while the IMF directions on both sides of the TD lie parallel to the discontinuity plane. As an entropy mode discontinuity, the TD convects with the solar wind flow velocity, with its normal direction $\mathbf{n} = (-0.50, 0.87, 0)$ in the xy plane, perpendicular to the IMF. We define time t = 0 as when the TD plane intersects the y = 0 axis at a distance corresponding to $x = 185\,R_E$.

LIN ET AL. 2 of 9



3. Simulation Results: Global Symmetry Breaking of HFAs and the Generation Mechanism

The interplanetary TD propagates anti-sunward and duskward into the domain, with its normal n at 60° relative to the -x direction. The discontinuity first touches the bow shock on the dawnside at t=2360 s, where it lies tangent to the local bow shock front. Little interaction between the TD and the bow shock is seen in the early period, as the TD normal is largely parallel to the shock normal so the TD moves too fast along the shock to allow any significant interaction (Lin, 2002; Schwartz et al., 2000). More significant features appear as the TD moves to the subsolar region. Figure 1 shows contour plots of ion density N in (a) the y=0 and z=-5 R_E planes at t=2735 s, (b) y=8.5 R_E and z=-5 R_E at t=3018 s, and (c) y=10 R_E and z=-5 R_E at t=3395 s, together with the typical magnetic field lines. At t=2735s, the y=0 plane cuts through the thin TD (with half-width of ~ 0.13 R_E) at x=14.5 R_E , as marked by "TD" in Figure 1a. The IMF changes from $\mathbf{B}_0=(3.0, 1.7, 0)$ nT ahead of the TD (duskside) to point purely southward on the trailing side. There is only a slight density perturbation attending this directional TD. The density increases as the solar wind plasma crosses the bow shock (at a standoff distance of ≈ 13 R_E and labeled as "BS" in Figure 1a). It is considerably lower within inside the magnetopause (at a standoff distance of ≈ 9.9 R_E and labeled as "MP" in Figure 1a). The orthospiral IMF with $B_{z0}=0$ results in a Q- $\|$ shock around the dusk side equatorial region, as seen from the significant density ripples and field-aligned filaments in the foreshock.

At t = 3018 s, the interaction of the TD with the subsolar bow shock has resulted in the formation of an HFA inside the TD, as marked in Figure 1b. A significant density decrease is present in the HFA, developed along the TD from the BS-TD intersection. At t = 3395 s, the TD has further propagated duskward, and the HFA cavity has expanded significantly and is elongated further southward, with a thickness $\sim 10 R_E$ (See Movie S1 in Supporting Information S1 for the time evolution.) The magnetopause erodes by $\sim 1.5 R_E$ behind the TD in response to the IMF variation. An immediately noticeable result is that the HFA appears only south of the equator although the IMF has a north-south symmetry on both sides of the TD. As the TD propagates tailward, it causes significant pressure perturbations and distortions on the southern magnetopause (C. P. Wang et al., 2021b).

Figure 2a depicts density structures in the planes of $z = +20 R_E$, 0, and $-20 R_E$ at t = 3772 s. The HFA in the southern hemisphere extends about $40 R_E$ far upstream into the solar wind from the magnetosheath, whereas at $z = +20 R_E$ there is no HFA but only a thin TD together with foreshock waves on the leading (Q-||) side. The north-south asymmetry of the HFA is further shown in Figure 2b, which plots the density contours in the TD plane (marked in Figure 2a) perpendicular to the equator. The density drop associated with the HFA starts just southward from z = 0. Some foreshock perturbations are also seen around the subsolar region.

The spatial profiles of various quantities as a function of x through the HFA is shown in Figure 2c, along the blue solid path marked in the z=-20 R_E plane in Figure 2a, from (x,y,z)=(-2,20,-20) R_E on the leading (anti-sunward) side to (-13,30,-20) R_E . Yellow shading highlights the core of the HFA, where the IMF changes direction through the much widened TD. On the leading side, the IMF has finite B_x and B_y , with B_z fluctuating about zero. Correspondingly, the electric field, dominated by the convection field $-\mathbf{V}_x \times \mathbf{B}_y$, is in the \mathbf{E}_z direction parallel to the TD front. On the trailing side of the shaded HFA, the IMF has turned to $B_z=-3.4$ nT. The electric field is dominated by $E_y=+1.36$ mV/m, and thus a normal component of 1.18 mV/m into the TD. In the core region of this strong HFA, the magnetic field strength almost diminishes to zero. The solar wind speed is reduced by more than 50%, with a significant flow deflection. The ion temperature is enhanced dramatically in both T_{\parallel} and T_{\perp} , with $T_{\parallel} > T_{\perp}$ ($T_{\perp} > T_{\parallel}$) toward the trailing (leading) side. A compression with enhanced density bounds either side of the HFA core.

The electric field on the trailing side, $E_y > 0$ pointing toward the TD, is expected to contribute to the HFA generation. Since this electric field is the same both northward and southward of the equator, one might naturally expect the HFA to form at all latitudes. However, our 3-D results clearly demonstrate that the HFA only forms in the southern hemisphere (z < 0). Such a striking global north-south asymmetry exists even though the IMF is symmetric in z on either side of the interplanetary TD.

To understand the mechanism that leads to the global symmetry breaking of the HFA, we now investigate the ion dynamics in the interaction. The left column of Figure 3 shows the contours of B in the y = 0 plane at t = 2792 s, when the TD has arrived the subsolar region. The striking asymmetry in the HFA can be seen in the contour plot: the HFA cavity exists only in the southern hemisphere, whose center is marked by the pink dashed line in z < 0,

LIN ET AL. 3 of 9

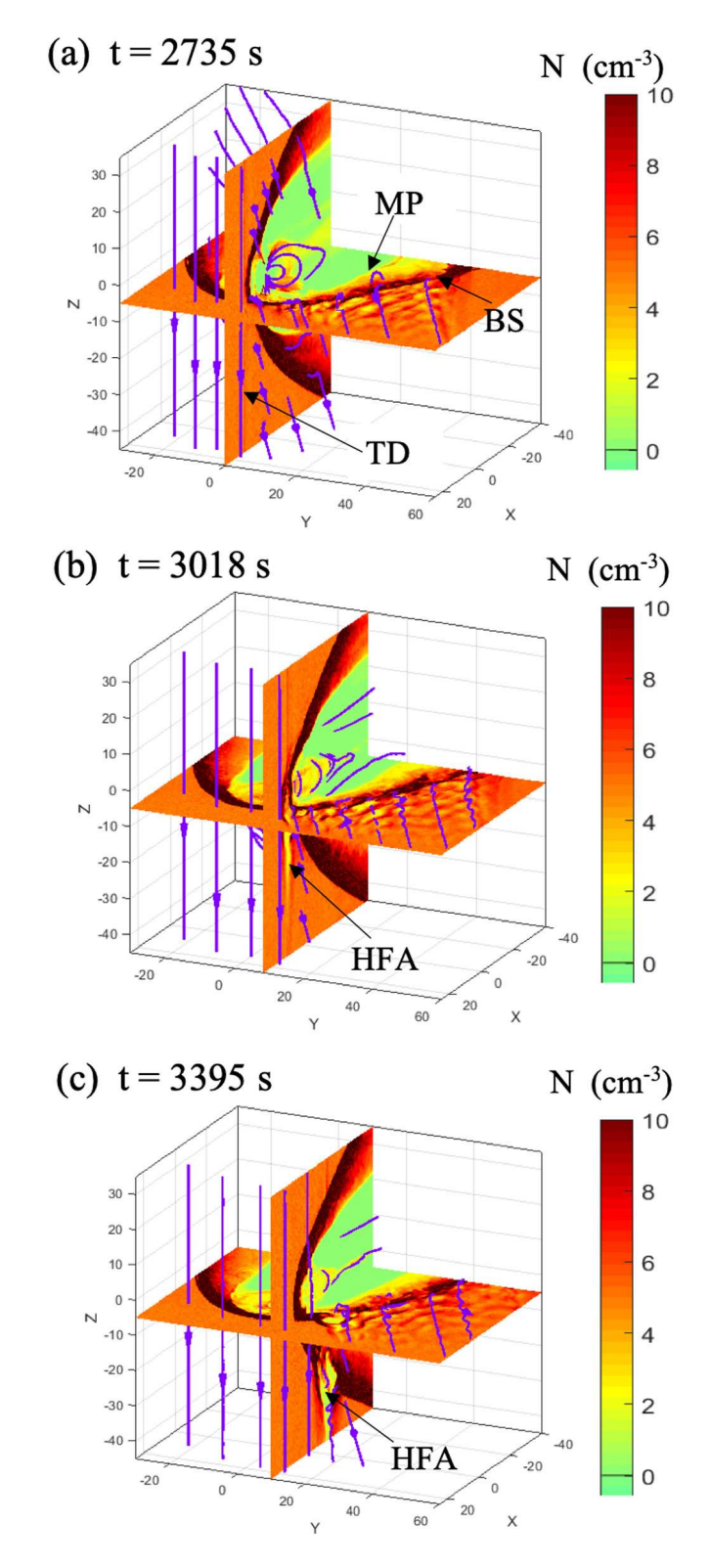


Figure 1. Ion density (N) contours in (a) the y = 0 & z = -5 R_E planes at t = 2735 s, (b) y = 8.5 R_E & z = -5 R_E at t = 3018 s, and (c) y = 10 R_E & z = -5 R_E at t = 3395 s obtained from the hybrid simulation show the generation of hot flow anomalies (as indicated) in z < 0 by the tangential discontinuity-bow shock interaction. The violet solid lines are magnetic field lines, and labels "BS" and "MP" mark the bow shock and magnetopause, respectively.

LIN ET AL. 4 of 9

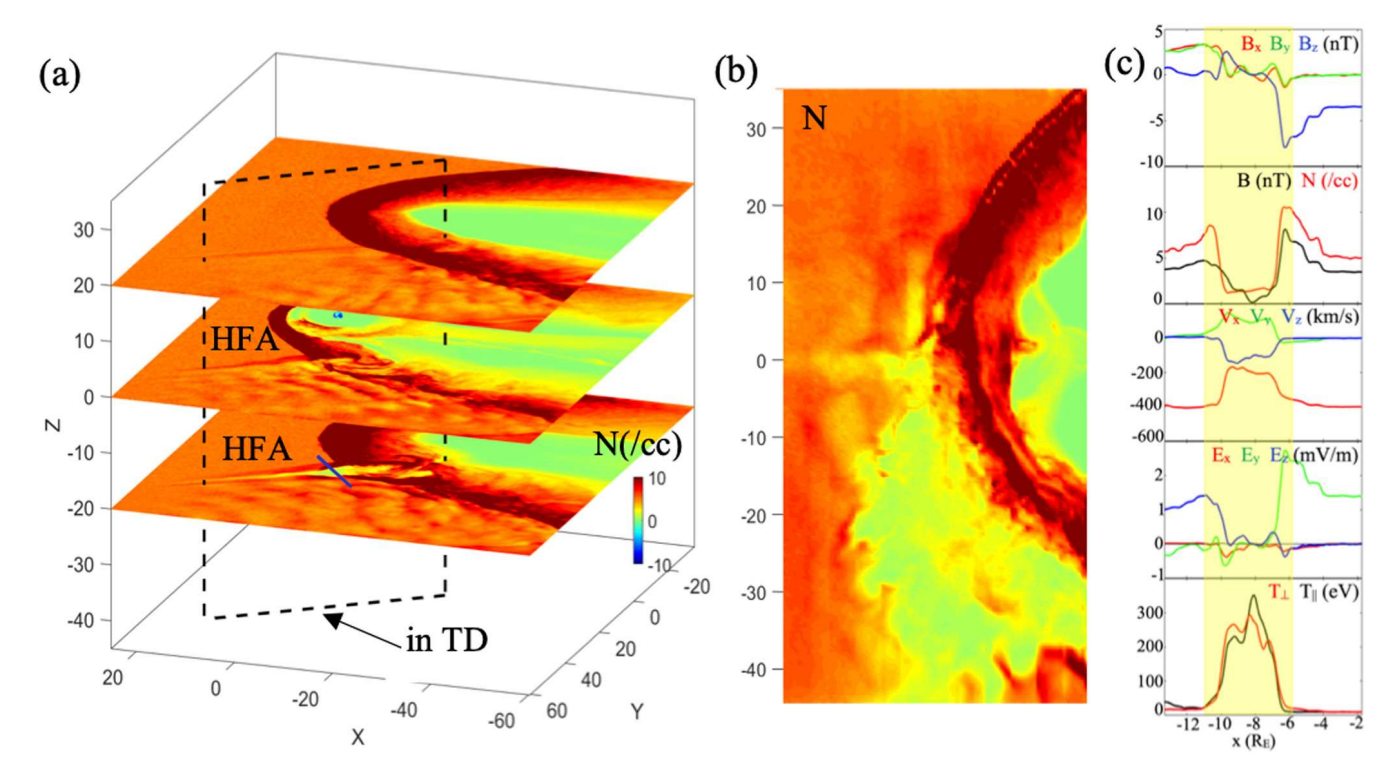


Figure 2. (a) Ion density N at $z = +20 R_E$, 0, and $-20 R_E$ at t = 3772 s show the presence of hot flow anomaly (HFA) southward of the equator (z < 0 only) along the tangential discontinuity (TD). (b) Density contours in the rectangular plane in Figure 2a inside the TD illustrate the north-south asymmetry of HFA. (c) Spatial profiles of various quantities as a function of x through the HFA along the solid path marked in the $z = -20 R_E$ plane in Figure 2a, with yellow shading highlighting the HFA core.

whereas the thin TD (marked by the pink dashed line in z > 0) is well maintained in the northern hemisphere. The right two columns of Figure 3 show the ion distributions at four locations "a", "b", "c", and "d" (marked in the contour plot of B) around the TD-bow shock intersection at t = 2792 s. There are about 20-100 particles per cell, and 25,000-79,000 particles in each distribution plot from a box of size $\Delta x \times \Delta y \times \Delta z \simeq 5d_{i0} \times 20d_{i0} \times 10$ d_{i0} . This number of particles more than suffices to capture the foreshock physics. In the following, we show how differing ion distributions at these locations around the HFA or TD, both north and south of the equator, provide important clues concerning the cause of the striking asymmetry.

The top row in the right two columns of Figure 3 shows the ion velocity $(v_{ix} - v_{iy})$ and $v_{ix} - v_{iz}$ distributions at point "a" on the trailing side of the HFA in the southern hemisphere, where the IMF is dominated by B_z and the shock is Q- \perp . The cold solar wind population around $v_{ix} \simeq -400$ km/s, marked as "SW", is being slowed down while entering the enhanced magnetic field of the shock. The decelerated ions are deflected dawnward as they follow a left-hand gyration orbit around the negative B_z , and then specularly reflected (turned to $v_{iy} > 0$) by the shock, following the sequence 1-2-3 marked in the $v_{ix} - v_{iy}$ plot. Meanwhile, the gyrating ions are accelerated duskward (with the gyro-center shifted to $v_{iv} > 0$) toward the HFA by $E_v > 0$. The distribution attains a maximum v_{iv} of ~550 km/s, which results in a significant normal velocity up to 700 km/s pointing into the TD, as seen in row "a", where the pink dashed line shows the orientation of the TD plane. Considering the normal convection speed of TD, $V_{\rm TD} \sim 200$ km/s, the gyrating beam possesses an inward velocity up to 500 km/s relative to the TD. Moreover, the TD front moves along the subsolar shock surface with speed $V_{\rm TD}/\cos 30^{\circ} \sim 231$ km/s (roughly in the +y direction), slower than in the flank region. The TD travels a distance of $\sim 21d_{10}$ in half the particle gyro period, comparable to the diameter of the gyro orbits $(\sim 20d_n)$ of particles that are initiated outside the HFA. The reflected ion beam can therefore be effectively accumulated in the TD, consistent with the HFA occurrence when the TD approaches the subsolar area. A reflected ion beam is also seen at location "b" inside the HFA (row "b" in Figure 3), but the ion acceleration in +y is weakened because of the reduced $lB_{s}l$. An obvious southward $v_{is} < 0$ is gained by the reflected beam at this point further southward of the equator (which we will further elaborate in the discussion for point "c").

LIN ET AL. 5 of 9

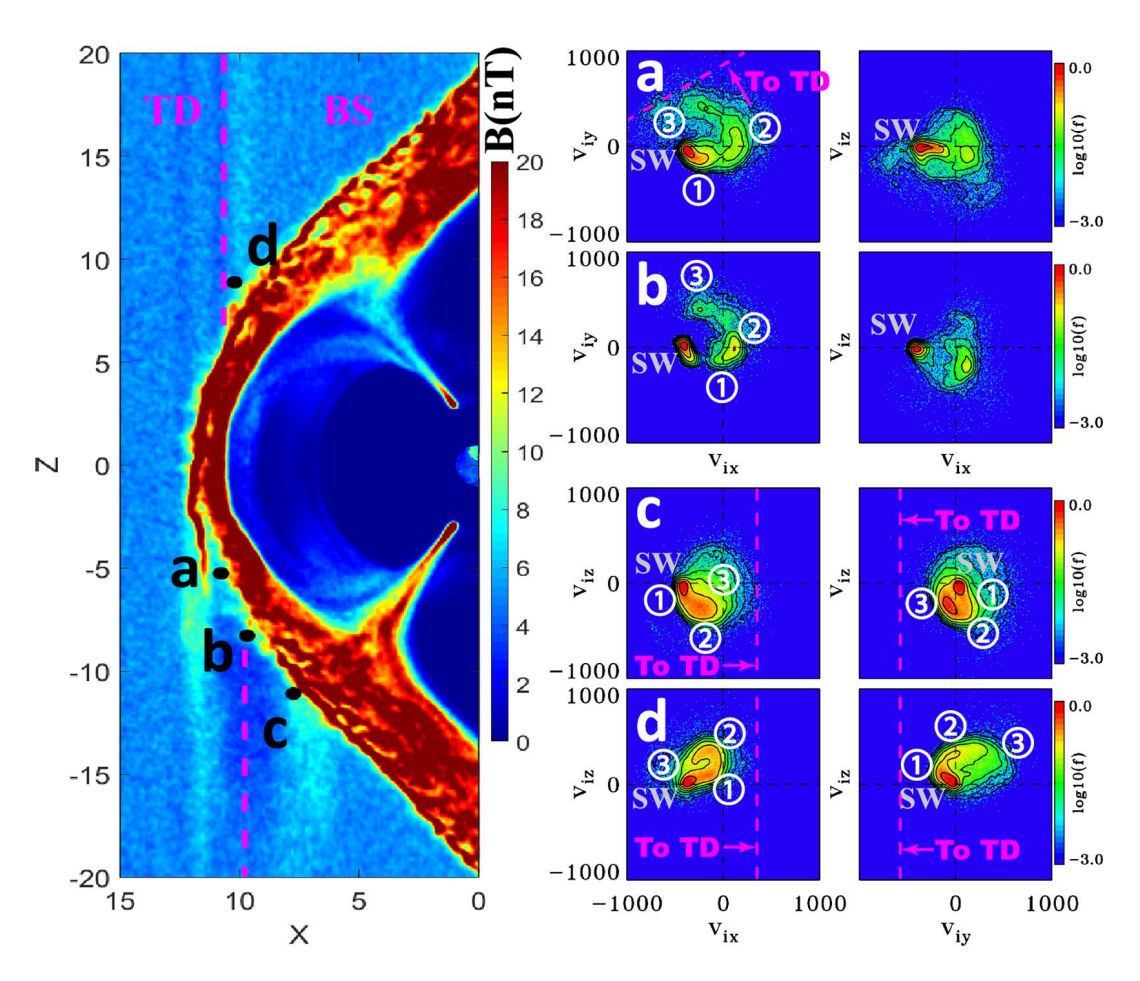


Figure 3. Ion kinetic structure illustrating the mechanism for global asymmetry of hot flow anomaly (HFA) (Left) Magnetic field contours at y = 0 around the dayside bow shock (BS), with the dashed line indicating the center of tangential discontinuity (TD) (z > 0) or HFA (z < 0), at t = 2792 s (Right) Ion velocity (in units of km/s) distributions at t = 2792 s, at four locations "a", "b", "c", and "d" (marked in the left plot) around the TD-BS intersection are plotted in rows a, b, c, and d, respectively. The cold solar wind ion beam is marked as "SW". On the trailing side of the TD, the IMF points due southward and distributions of reflected ions similar to those in row "a" are observed both north and south of the equator. The gyrating ion beams are accelerated duskward (+y, into TD). On the leading side with a sunward and duskward IMF, different distributions of reflected ions are observed north and south of the equator ("c" and "d"), with reflected distributions moving duskward (away from TD) north of the equator and dawnward (into TD) south of the equator. No HFA is formed north of the equator. The pink arrows indicate the normal velocity directions toward the TD plane (pink dashed lines). The circled numbers mark the sequence 1-2-3 for the ion gyration direction.

Figure 4 sketches the ion orbits in the bow shock-TD interaction. Assuming the solar wind is cold for simplicity, a solar wind ion incident along the -x direction and hitting the southern bow shock on the trailing side (side 1) of the TD is sketched by the orange ion trajectory for z < 0. As the ion is reflected by the bow shock, it gyrates in the xy plane around the southward \mathbf{B}_1 while being accelerated inward by the duskward (green) \mathbf{E}_1 . Such ion acceleration by \mathbf{E}_1 works the same for the northern hemisphere, as sketched by the identical orange ion trajectory for z > 0. The ion distribution on the trailing side similar to that at "a" is observed both north and south of the equator.

Row "c" of Figure 3 plots the $v_{ix} - v_{iz}$ and $v_{iy} - v_{iz}$ distributions at point "c" at the leading edge of the HFA, where the IMF lies in the $B_x - B_y$ plane and the electric field points to E_z . The initial solar wind ions are being slowed down in v_{ix} and reflected at the Q-|| shock. Since point "c" is southward from the equator (at $z = -11.5 R_E$), the originally sunward and duskward IMF lines gain a northward component across the shock in the magnetosheath (See the field line geometry relative to the shock normal, \hat{n}_{BS} , in the southern hemisphere in Figure 4). As the solar wind ions encounter the shock front, their velocities turn to $v_{iz} < 0$ due to the instantaneous parallel velocity along the field lines. Thus, the particles encountering the shock are initially decelerated in $|v_{ix}|$ but quickly gain a southward velocity component. Such a southward kick of the ion velocity by the shock causes their gyration

LIN ET AL. 6 of 9

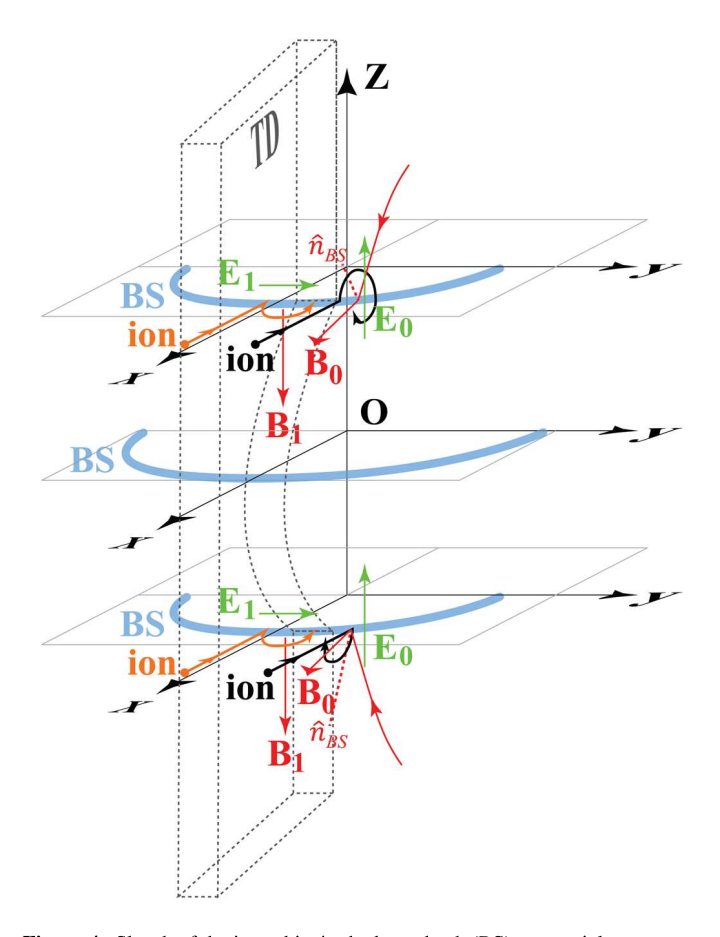


Figure 4. Sketch of the ion orbits in the bow shock (BS)-tangential discontinuity (TD) interaction. The part of the TD upstream of the bow shock, oriented at 30° from the x axis and perpendicular to the xy plane, is shown as the dashed plate, and the BS transitions are shown as thick blue curves for z = 0 and two planes in z > 0 and z < 0. The IMF changes from \mathbf{B}_0 (lies in the xy plane) on the leading side of the TD to \mathbf{B}_1 (pointing southward) on the trailing side, and \hat{n}_{BS} indicates the local shock normals. The orange solar wind ions (assumed cold) hit the bow shock on the trailing side (side 1) in the z > 0and z < 0 planes. They gyrate in the xy plane around \mathbf{B}_1 after being reflected by the shock and are accelerated into the TD by duskward electric field \mathbf{E}_1 . On the leading side, while the incident ions (black) are slowed down and reflected near the shock transition, they gyrate around \mathbf{B}_0 after gaining the downstream velocities northward (in z > 0) and southward (in z < 0) because of the opposite field line bending on the two sides of the equator. Correspondingly, the gyration is away from (into) the TD in the northern (southern) hemisphere, and the gyro orbits are skewed duskward due to the northward electric field

orbits (skewed by the positive E_z) shown in row "c" of Figure 3 to follow the sequence 1-2-3 (turning to $v_{iy} < 0$) around the sunward and duskward magnetic field. Normal speeds, dominated by v_{iy} , up to ~300 km/s are seen toward the TD (left plot of Row "c"), corresponding to an inward speed of ~500 km/s relative to the TD. As a result, a significant portion of ions within ~gyro diameter distance are injected into the TD from the leading side, even though there exists no normal electric field. The trajectory of a typical ion on the leading side in z < 0 is sketched as a black ion in Figure 4. Once the particle gyrates about a half of the circular orbit into the TD, it participates in the plasma interaction that leads to the plasma heating and formation of the HFA. The ion orbits at locations "a", "b", and "c" demonstrate that ion beams are accumulated into the TD from both sides, leading to a significant plasma heating and thus a strong HFA in the southern hemisphere.

The results at point "c" in Figure 3 indicate that the negative v_{iz} of the reflected ions at the leading edge drives an inward gyration to the TD, enhances plasma pressures within the HFA, and thus enhances the strength of the HFA. Location "d" is also on the leading side of the TD. But since this point is northward of the equator (at $z = +8.5 R_E$), when the solar wind ions encounter the bow shock, their v_{iz} turns from nearly zero to positive (row "d" in Figure 3) following the bending of the field lines opposite to that at point "c". Thus, the slowed down and reflected ions first gain northward speeds (with a slight turn to v_{iv} due to the field line tilt in y), and then turn duskward ($v_{iv} > 0$) as they gyrate in the sunward and duskward IMF (following the sequence 1-2-3 in row "d" of Figure 3). By contrast to its counterpart ahead of the TD in the southern hemisphere, these ions move away from the discontinuity (opposite to the pink arrow directions in row "d") and cannot participate in HFA formation. The trajectory of a typical ion on the leading side of the TD in the northern hemisphere is sketched as a black ion in Figure 4 for z > 0, with its initial gyro phase corresponding to a mainly northward velocity and thus an outward circular orbit. The orbit is skewed due to the existence of $E_{70} > 0$ such that the gyro center moves duskward with a speed of ~250 km/s (estimated by the $\mathbf{E} \times \mathbf{B}$ drift), comparable to the duskward TD speed (~231 km/s) on the shock front. The net result is that the reflected particle gyrates mainly outside the TD. In the bottom right plot of Figure 3, the outward gyrating particles in the distribution are seen to be scattered by the shock before they complete a full gyro orbit. Since the thickness of the TD ($\sim d_{10}$) \ll the Larmor radius ($\sim 10d_{10}$), the majority of the reflected particles in and at the edge of the TD gyrates outside.

Therefore, although ions are injected into the TD on the trailing side by $E_y > 0$, similar to the southern hemisphere, a significant portion of them are removed from the TD on leading side, and the accumulation or counter-streaming beam interaction occurring at location "c" can barely exist at location "d". As a result, no HFA is generated in the northern hemisphere.

4. Summary and Discussion

In summary, our global hybrid simulation for the TD-bow shock interaction is shown for a case in which the TD normal lies in the equatorial (z = 0) plane. It is demonstrated that although the IMF in the solar wind is symmetric about the equator on both sides of the TD, a global north-south asymmetry of the HFA is present owing to the 3-D physics. (a) Although the convection electric field points into the TD from the trailing side of the discontinuity on both sides of the equator, the HFA is generated only in the southern hemisphere. (b) The generation of the HFA results from bow shock-reflected ions energized by the inward-pointing electric field on the trailing side of the TD and inward ion gyration in the B field on the leading side, while the latter phenomenon of inward motion

LIN ET AL. 7 of 9



only occurs south of the equator due to the global bow shock geometry. (c) The global north-south symmetry breaking of HFA is driven by a reversal in the north-south (ν_{iz}) component of the ion velocities at the bow shock in the two hemispheres, such that on the leading side the ions gyrate into (away from) the TD in the southern (northern) hemisphere.

Our study shows that in 3-D, global capacity, a mechanism associated with the gyro-orbits of reflected ions leads to enhanced or depressed ion accumulation in the TD. In some regions, such an ion beam adds to the conventional acceleration mechanism by convection electric field, leading to a strong HFA with a vanishing core magnetic field strength (Figure 2c). In some other regions, however, the ion beams lead to the disappearance of the HFA, although there exists an inward convection electric field on one side.

The mechanism presented in this paper indicates that HFAs must generally exhibit north-south and dawn-dusk asymmetries depending on the orientation of the IMF discontinuity that produces them, although only one case is presented to illustrate the basic concept. A similar run with the IMF geometry rotated by 90° systematically about the Sun-Earth line shows the global asymmetry exists in the same way but in the dawn-dusk direction. It would be interesting to determine how the 3-D physics controls the strength of HFAs latitudinally and longitudinally in cases with general IMF orientations, for example, by statistical studies (Chu et al., 2017; Facskó et al., 2009), and identify how the global structure of HFAs depends on the solar wind and IMF parameters.

Data Availability Statement

Results in this paper are generated from our computer simulation code as described in Section 2. The numerical data used for generating the presented figures are available via https://doi.org/10.6084/m9.figshare.15167061.

Acknowledgments

This work is supported by NASA (Grants NASA-80NSSC20K1322 and NASA-80NSSC19K0840) and NSF EPSCOR (Grant OIA-1655280) to Auburn University. C. P. Wang is supported by NASA-80NSSC19K0840. S. Lee and D. G. Sibeck are supported by NASA HSR Program WBS 791926.02.09.01.58. Computer resources are provided by NASA NAS Division.

References

- Archer, M. O., Horbury, T. S., & Eastwood, J. P. (2012). Magnetosheath pressure pulses: Generation downstream of the bow shock from solar wind discontinuities. *Journal of Geophysical Research*, 117, A05228. https://doi.org/10.1029/2011JA017468
- Burgess, D. (1989). On the effect of a tangential discontinuity on ions specularly reflected at an oblique shock. *Journal of Geophysical Research*, 94, 472–478. https://doi.org/10.1029/ja094ia01p00472
- Cheng, L., Lin, Y., Perez, J. D., Johnson, J. R., & Wang, X. (2020). Kinetic alfvén waves from magnetotail to the ionosphere in global hybrid simulation associated with fast flows. *Journal of Geophysical Research*, 125, e2019JA027062. https://doi.org/10.1029/2019JA027062
- Chu, C., Zhang, H., Sibeck, D., Otto, A., Zong, Q., Omidi, N., & Angelopoulos, V. (2017). Themis satellite observations of hot flow anomalies at earth's bow shock. *Annals of Geophysics*, 35(3), 443. https://doi.org/10.5194/angeo-35-443-2017
- Delamere, P. (2006). Hybrid code simulations of the solar wind interaction with comet 19p/borrelly. *Journal of Geophysical Research*, 111, A12217. https://doi.org/10.1029/2006ja011859
- Eastwood, J., Sibeck, D., Angelopoulos, V., Phan, T., Bale, S., & McFadden, J. (2008). THEMIS observations of a hot flow anomaly: Solar wind, magnetosheath, and ground-based measurements. *Geophysical Research Letters*, 35(17), L17S03. https://doi.org/10.1029/2008gl033475
- Facskó, G., Kecskeméty, K., Erdős, G., Tátrallyay, M., Daly, P. W., & Dandouras, I. (2008). A statistical study of hot flow anomalies using Cluster data. Advances in Space Research, 41, 1286–1291. https://doi.org/10.1016/j.asr.2008.02.005
- Facskó, G., Németh, Z., Erdős, G., Kis, A., & Dandouras, I. (2009). A global study of hot flow anomalies using Cluster multi-spacecraft measurements. *Annales Geophysicae*, 27, 2057–2076. https://doi.org/10.5194/angeo-27-2057-2009
- Hasegawa, H., Zhang, H., Lin, Y., Sonnerup, B. U. Ö., Schwartz, S. J., Lavraud, B., & Zong, Q.-G. (2012). Magnetic flux rope formation within a magnetosheath hot flow anomaly. *Journal of Geophysical Research*, 117, A09214. https://doi.org/10.1029/2012JA017920
- Jacobsen, K., Phan, T., Eastwood, J., Sibeck, D., Moen, J., & Angelopoulos, V. (2009). THEMIS observations of extreme magnetopause motion caused by a hot flow anomaly. *Journal of Geophysical Research*, 114(A8), A08210. https://doi.org/10.1029/2008ja013873
- Lin, Y. (1997). Generation of anomalous flows near the bow shock by its interaction with interplanetary discontinuities. *Journal of Geophysical Research*, 102(A11), 24265–24282. https://doi.org/10.1029/97JA01989
- Lin, Y. (2002). Global hybrid simulation of hot flow anomalies near the bow shock and in the magnetosheath. *Planetary and Space Science*, 50(5–6), 577–591. https://doi.org/10.1016/s0032-0633(02)00037-5
- Lin, Y., Swift, D. W., & Lee, L. C. (1996). Simulation of pressure pulses in the bow shock and magnetosheath driven by variations in interplanetary magnetic field direction. *Journal of Geophysical Research*, 101(27), 251. https://doi.org/10.1029/96ja02733
- Lin, Y., Wang, X. Y., Lu, S., Perez, J. D., & Lu, Q. (2014). Investigation of storm-time magnetotail and ion injection using three-dimensional global hybrid simulation. *Journal of Geophysical Research A: Space Physics*, 119(9), 7413–7432. https://doi.org/10.1002/2014JA020005
- Lin, Y., Wing, S., Johnson, J. R., Wang, X. Y., Perez, J. D., & Cheng, L. (2017). Formation and transport of entropy structures in the magnetotail simulated in a 3-D global hybrid code. *Geophysical Research Letters*, 44, 5892–5899. https://doi.org/10.1002/2017GL073957
- Liu, T. Z., An, X., Zhang, H., & Turner, D. (2020). Magnetospheric multiscale observations of foreshock transients at their very early stage. *The Astrophysical Journal*, 902(1), 5. https://doi.org/10.3847/1538-4357/abb249
- Lucek, E. A., Horbury, T. S., Balogh, A., Dandouras, I., & Rème, H. (2004). Cluster observations of hot flow anomalies. *Journal of Geophysical Research*, 109(A18), 6207. https://doi.org/10.1029/2003JA010016
- Omidi, N., & Sibeck, D. G. (2007). Formation of hot flow anomalies and solitary shocks. *Journal of Geophysical Research*, 112(A11), 1203. https://doi.org/10.1029/2006JA011663
- Omidi, N., Zhang, H., Sibeck, D., & Turner, D. (2013). Spontaneous hot flow anomalies at quasi-parallel shocks: 2. Hybrid simulations. *Journal of Geophysical Research A: Space Physics*, 118(1), 173–180. https://doi.org/10.1029/2012JA018099

LIN ET AL. 8 of 9



- Paschmann, G., Haerendel, G., Sckopke, N., Moebius, E., & Luehr, H. (1988). Three-dimensional plasma structures with anomalous flow directions near the Earth's bow shock. *Journal of Geophysical Research*, 93, 11279–11294. https://doi.org/10.1029/ja093ja10p11279
- Schwartz, S. J. (1995). Hot flow anomalies near the Earth's bow shock. Advances in Space Research, 15(8–9), 107–116. https://doi.org/10.1016/0273-1177(94)00092-f
- Schwartz, S. J., Kessel, R. L., Brown, C. C., Woolliscroft, L. J. C., & Dunlop, M. W. (1988). Active current sheets near the earth's bow shock. Journal of Geophysical Research, 93, 11295–11310. https://doi.org/10.1029/ja093ja10p11295
- Schwartz, S. J., Paschmann, G., Sckopke, N., Bauer, T. M., Dunlop, M., Fazakerley, A. N., & Thomsen, M. F. (2000). Conditions for the formation of hot flow anomalies at Earth's bow shock. *Journal of Geophysical Research*, 105(A6), 12639–12650. https://doi.org/10.1029/1999JA000320
- Sibeck, D. G., Borodkova, N. L., Schwartz, S. J., Owen, C. J., Kessel, R., Kokubun, S., & Zastenker, G. N. (1999). Comprehensive study of the magnetospheric response to a hot flow anomaly. *Journal of Geophysical Research*, 104(A3), 4577–4594. https://doi.org/10.1029/1998JA900021
- Thomas, V. A., Winske, D., Thomsen, M. F., & Onsager, T. G. (1991). Hybrid simulation of the formation of a hot flow anomaly. *Journal of Geophysical Research*, 96, 11625. https://doi.org/10.1029/91ja01092
- Thomsen, M. F., Gosling, J. T., Fuselier, S. A., Bame, S. J., & Russell, C. T. (1986). Hot, diamagnetic cavities upstream from the earth's bow shock. *Journal of Geophysical Research*, 91(A3), 2961–2973. https://doi.org/10.1029/ja091ia03p02961
- Thomsen, M. F., Thomas, V. A., Winske, D., Gosling, J. T., Farris, M. H., & Russell, C. T. (1993). Observational test of hot flow anomaly formation by the interaction of a magnetic discontinuity with the bow shock. *Journal of Geophysical Research*, 98(A9), 15319–15330. https://doi.org/10.1029/93ja00792
- Wang, C.-P., Wang, X., Liu, T. Z., & Lin, Y. (2020). Evolution of a foreshock bubble in the midtail foreshock and impact on the magnetopause: 3-D global hybrid simulation. *Geophysical Research Letters*, 47(22), e2020GL089844. https://doi.org/10.1029/2020GL089844
- Wang, C.-P., Wang, X., Liu, T. Z., & Lin, Y. (2021a). A foreshock bubble driven by an IMF tangential discontinuity: 3D global hybrid simulation. Geophysical Research Letters, 48(9), e2021GL093068. https://doi.org/10.1029/2021GL093068
- Wang, C.-P., Wang, X., Liu, T. Z., & Lin, Y. (2021b). Impact of foreshock transients on the flank magnetopause and magnetosphere and the ionosphere. Frontiers in Astronomy and Space Sciences, 8, 160. https://doi.org/10.3389/fspas.2021.751244
- Wang, S., Zong, Q., & Zhang, H. (2013). Cluster observations of hot flow anomalies with large flow deflections: 2. Bow shock geometry at HFA edges. Journal of Geophysical Research A: Space Physics, 118(2), 418–433. https://doi.org/10.1029/2012JA018204
- Zhang, H., Sibeck, D. G., Zong, Q.-G., Gary, S. P., McFadden, J. P., Larson, D., & Angelopoulos, V. (2010). Time history of events and macroscale interactions during substorms observations of a series of hot flow anomaly events. *Journal of Geophysical Research*, 115, A12235. https://doi.org/10.1029/2009JA015180
- Zhang, H., Sibeck, D. G., Zong, Q.-G., Omidi, N., Turner, D., & Clausen, L. B. N. (2013). Spontaneous hot flow anomalies at quasi-parallel shocks: 1. Observations. *Journal of Geophysical Research A: Space Physics*, 118(6), 3357–3363. https://doi.org/10.1002/jgra.50376
- Zhao, L. L., Zhang, H., & Zong, Q. G. (2017). A statistical study on hot flow anomaly current sheets. *Journal of Geophysical Research A: Space Physics*, 122(1), 235–248. https://doi.org/10.1002/2016JA023319

LIN ET AL. 9 of 9